Electronic Supplementary Material (ESI) for Physical Chemistry Chemical Physics

Supporting Information of

Synthesis and Characterization of Poly-L-Leucine Initialized and Immobilized by Rehydrated Hydrotalcite. Understanding of the Stability and Interaction Nature.

Ronald-Alexander Miranda,[a,b] Elisabetta Finocchio,[c] Jordi Llorca,[d] Francisco Medina,[a,b] Gianguido Ramis,[c] Jesús E. Sueiras,[a,b] and Anna M. Segarra*[a,b]

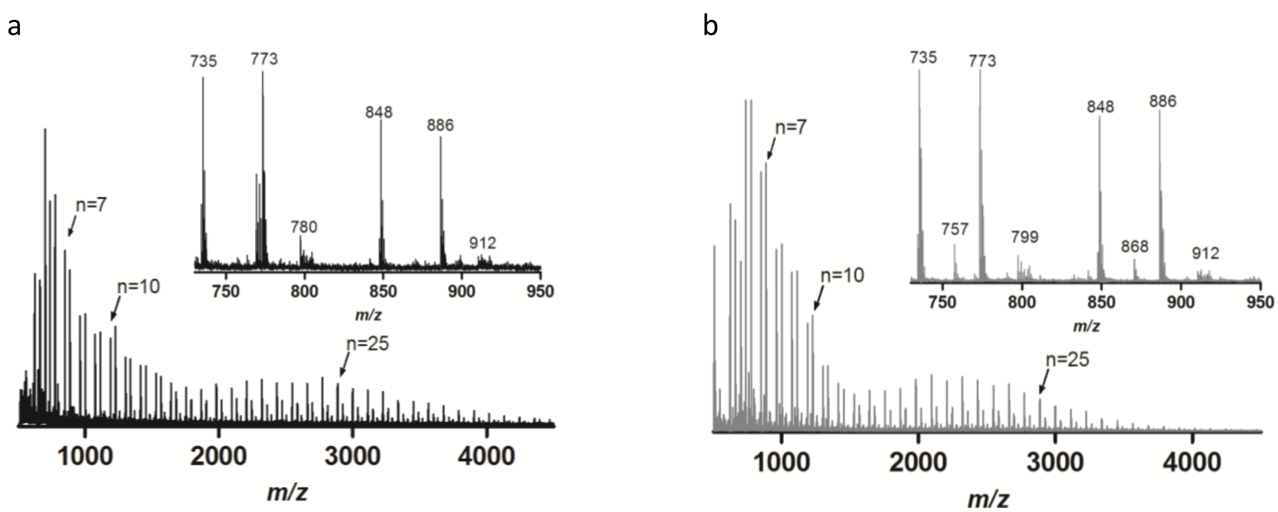

Figure S1 MALDI-TOF MS spectra of a) PLL2 and b) PLL3

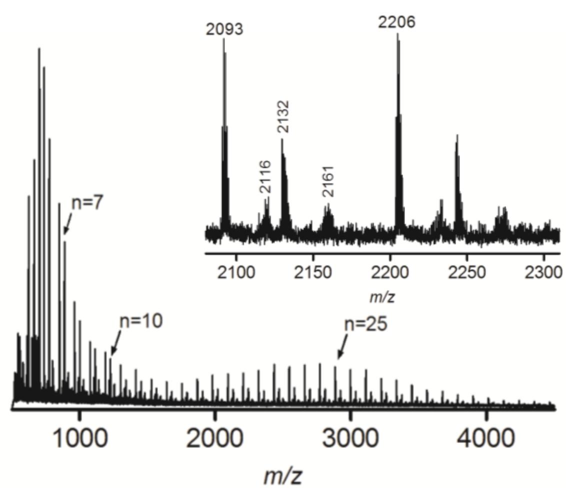

Figure S2 MALDI-TOF MS spectra of $PLL1_{60}$

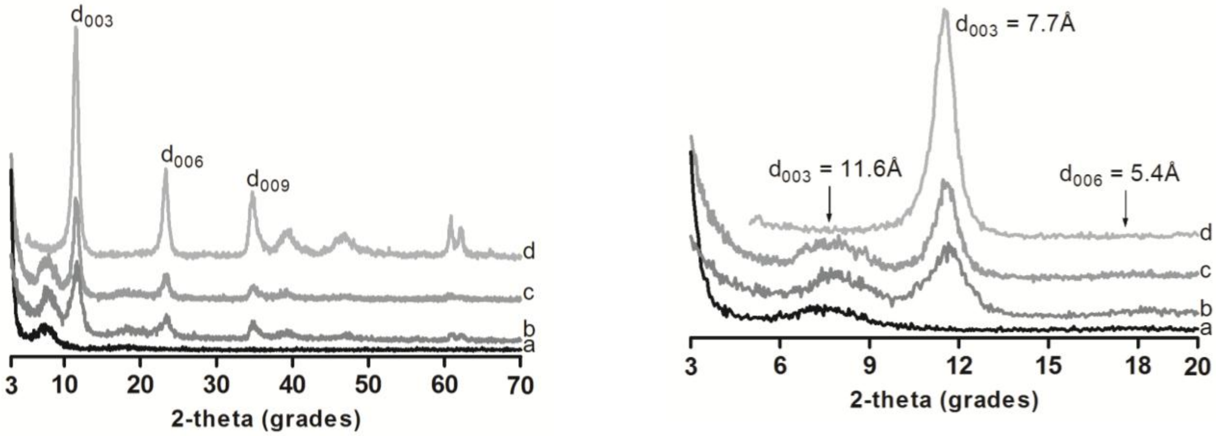

Figure S3 Left: XRD patterns of a) PLL3, b) IPL3, c) $IPL2_{60}$ and d) HT_{rus}. Right: XRD patterns in the 2θ range: 3-20º

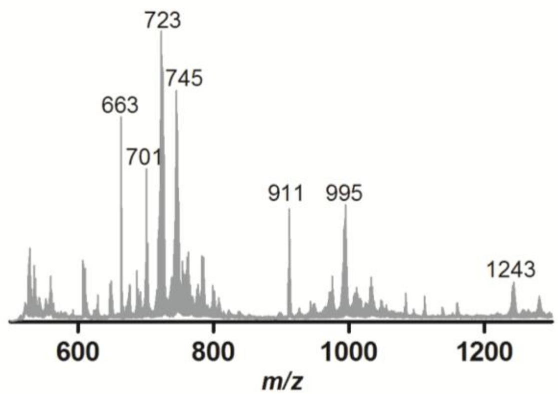

Figure S4 MALDI-TOF MS spectrum of HT_{rus}.

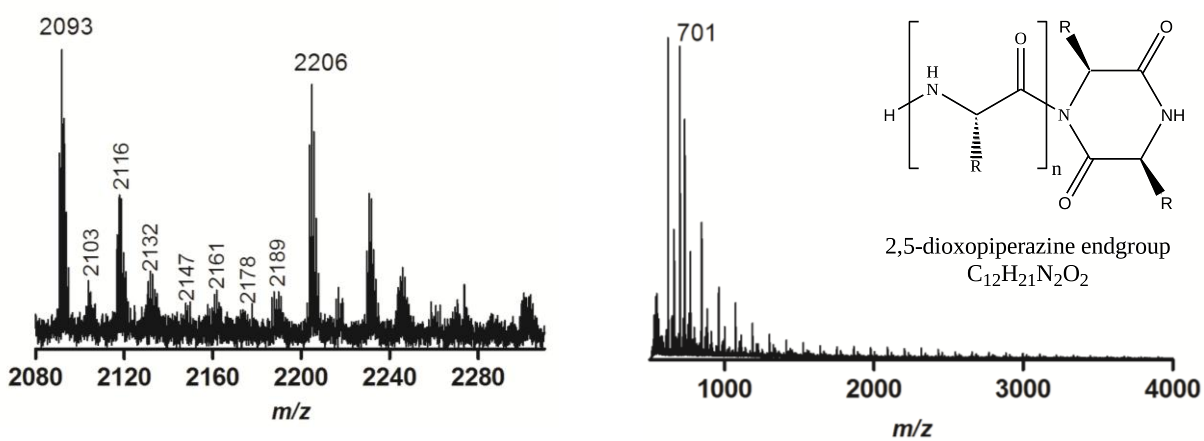

Figure S5 MALDI-TOF MS spectra of non-immobilized fraction of IPL3. Left: MALDI-TOF spectra in the m/z range: 2080-2310. Right: Entire spectra. See formation of $C_{12}H_{21}N_2O_2$ in W. N. E. van Dijk-Wolthuis, L. van de Water, P. van de Wetering, M. van Steenbergen, J. J. Kettenes-van den Bosch, W. Schuyl and

W. E. Hennink. Synthesis and characterization of poly-L-lysine with controlled low molecular weight .*Macromol. Chem. Phys.* **1997**, *198*, 3893.

a

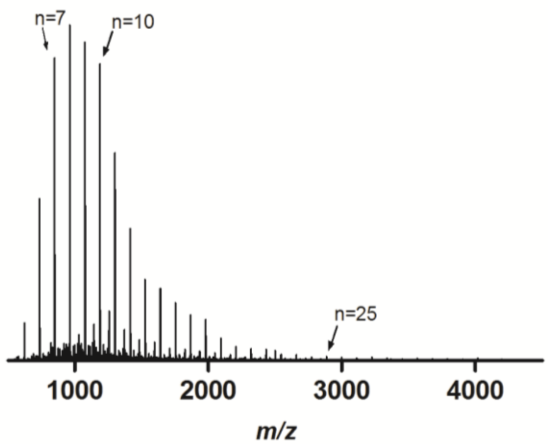

b

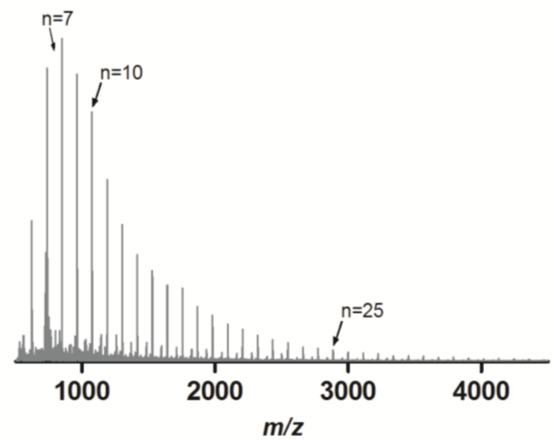

c

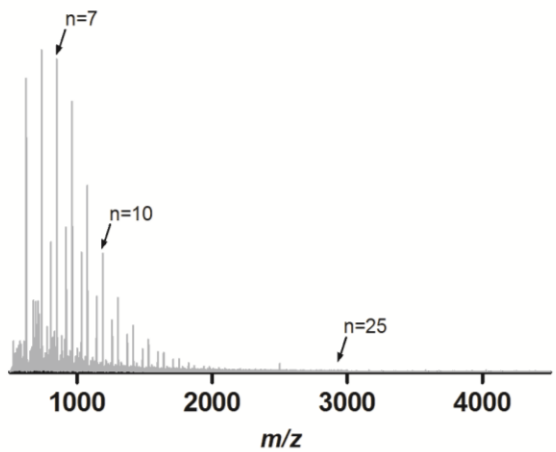

Figure S6 MALDI-TOF MS spectrum of a) PLL4, b) PLL5 and c) PLL6

Table S1 Calculated Masses (Da) of PLL4 by MALDI-TOF SM.

Endgroup	H/OH			H/NCA + 46Da	H/NCA		Cyclic	
DP	+ K^+	+ $2K^+$ - H^+	+ Na^+ [a]	+ K^+	+ K^+	+ H^+ - H_2O	+ H^+	+K^+
7	847	886	833	1030	988	931	793	831
8	960	999	946	1143	1101	1044	906	944
9	1073	1112	1058	1256	1214	1157	1019	1057
10	1186	1225	1171	1369	1327	1270	1132	1170
11	1299	1339	1284	1483	1441	1384	1245	1284
12	1413	1452	1397	1596	1554	1497	1358	1397

[a]Mass at 1171.8 is calculated as 10*Leu + H/OH + Na^+; nevertheless, it could be due to a cyclic polymer chain and calculated as 10*Leu + H/OH + K^+- H_2O.

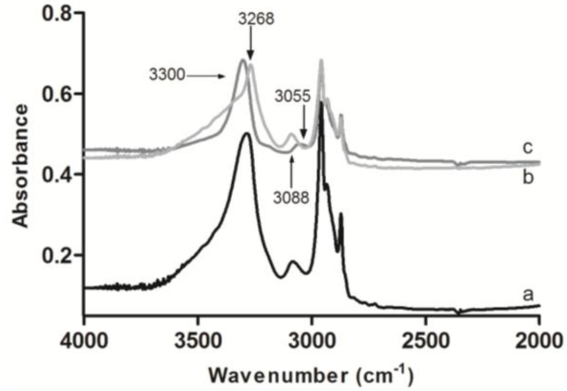

Figure S7 Skeletal FT-IR spectra of a) PLL4, b) Subtraction spectrum [PLL4 – PLL3] and c) PLL3 in the high frequency region.

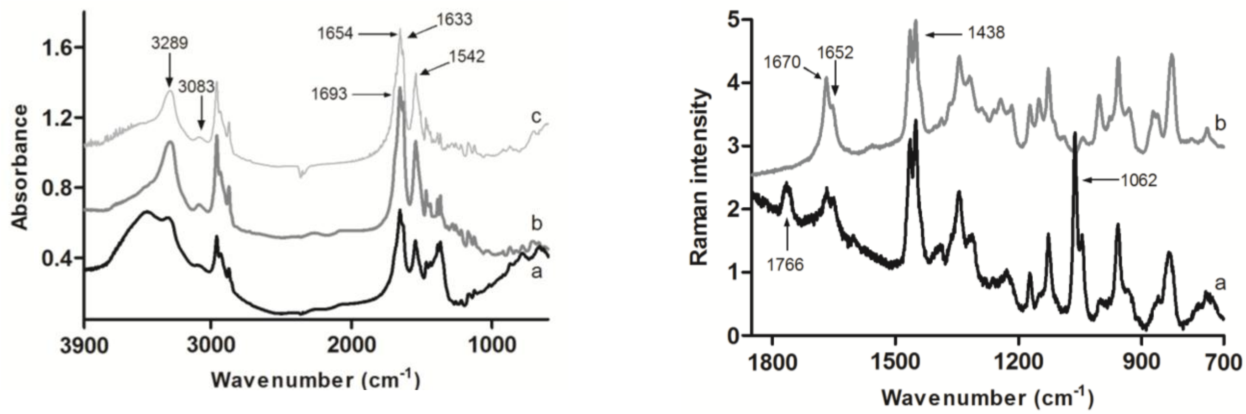

Figure S8 Skeletal FT-IR spectra (left) of a) PLL5, b) Subtracted spectrum [PLL6 – HT_{rus}] and c) PLL6. And Raman spectra (right) of a) PLL5 and b) PLL6.

a b c

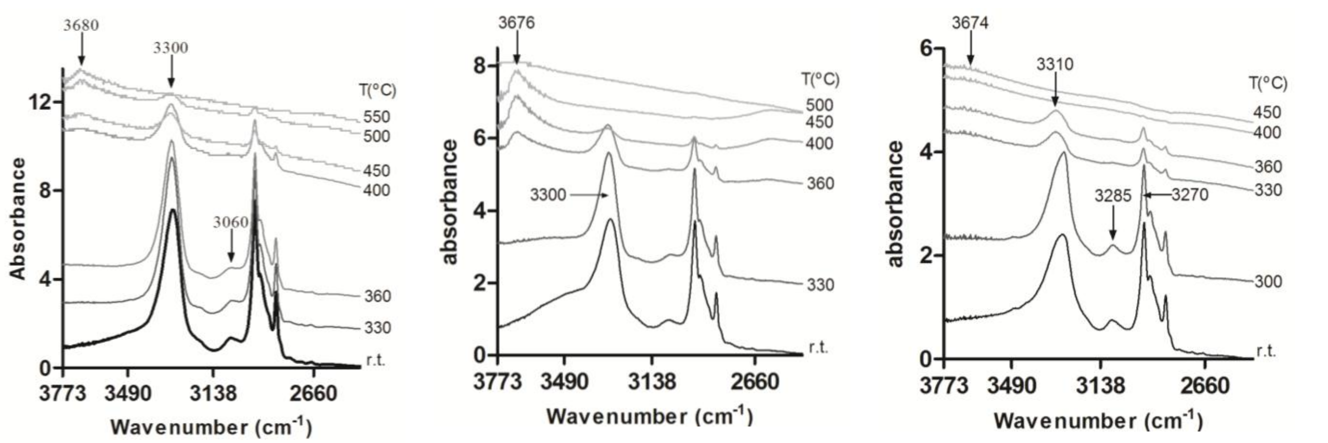

Figure S9 Skeletal FT-IR spectra in the higher frequency range of a) PLL3, b) $IPL2_{60}$ and c) PLL4 in KBr under outgassing conditions at increasing temperature

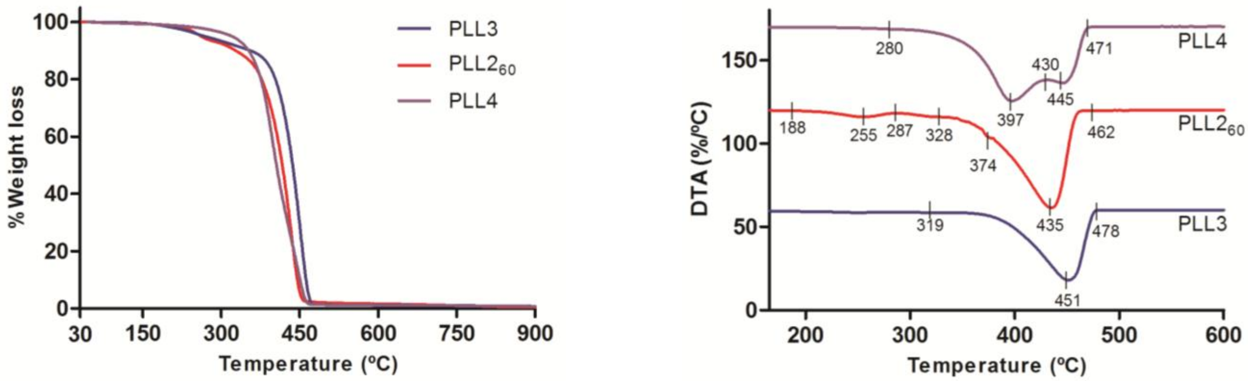

Figure S10 a) TG and b) DTA experiments of PLL3, $PLL2_{60}$ and PLL4

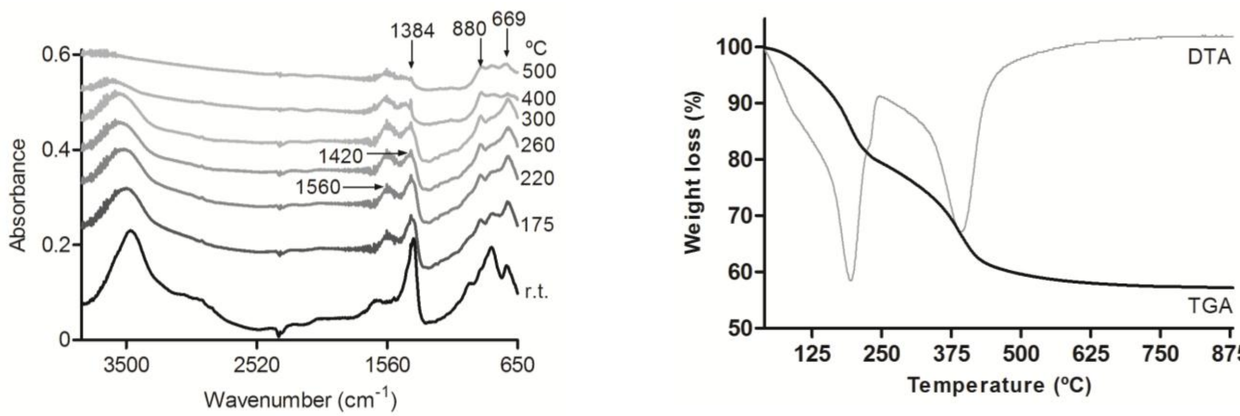

Figure S11 a) FT-IR at increasing temperature and b) TG/DTA experiment of HT_{rus}.

a b c

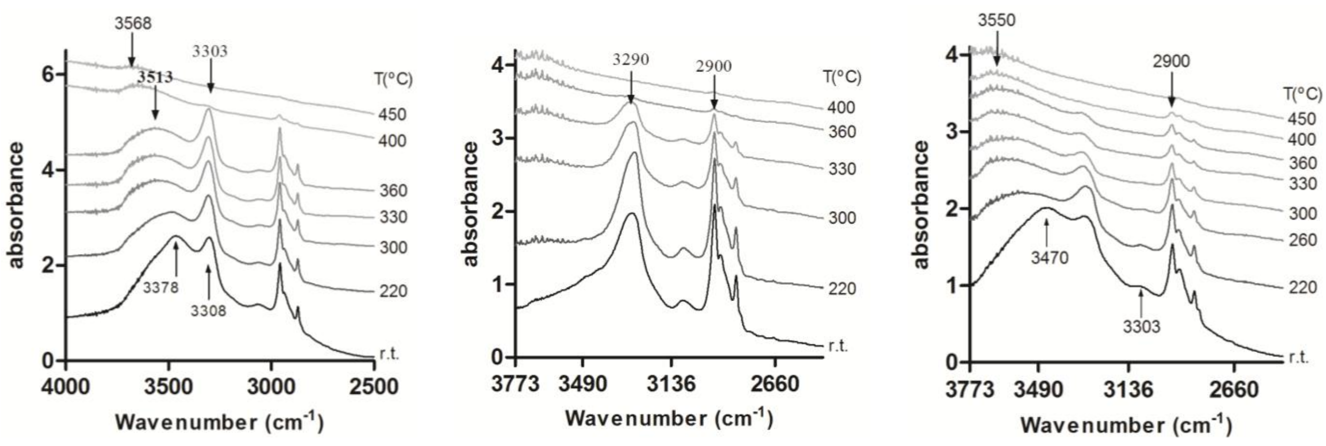

Figure S12 Skeletal FT-IR spectra in the higher frequency range of a) IPL3, b) PLL5 and c) PLL6 in KBr under out-gassing conditions at increasing temperature

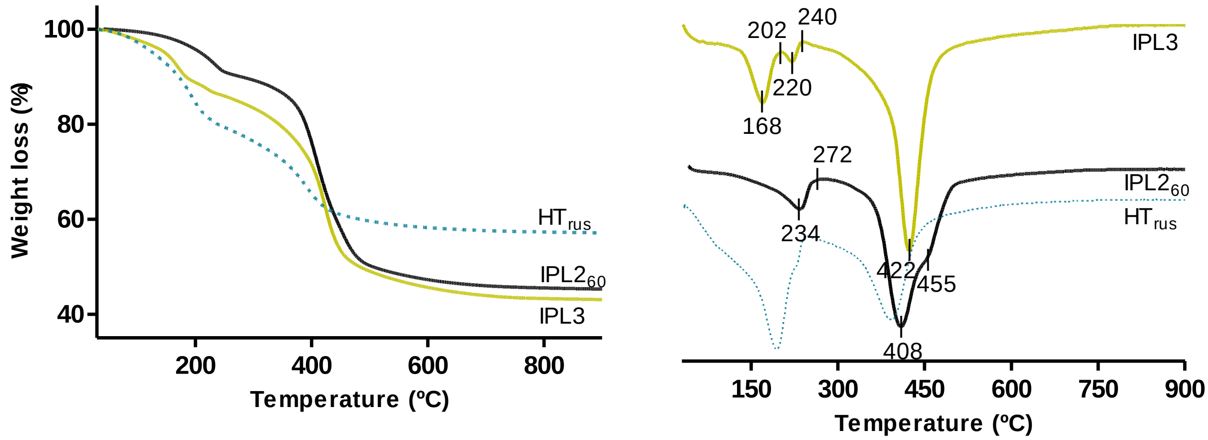

Figure S13 a) TG and b) DT analyses of IPL3 and IPL2$_{60}$. HTrus is showed as a reference.

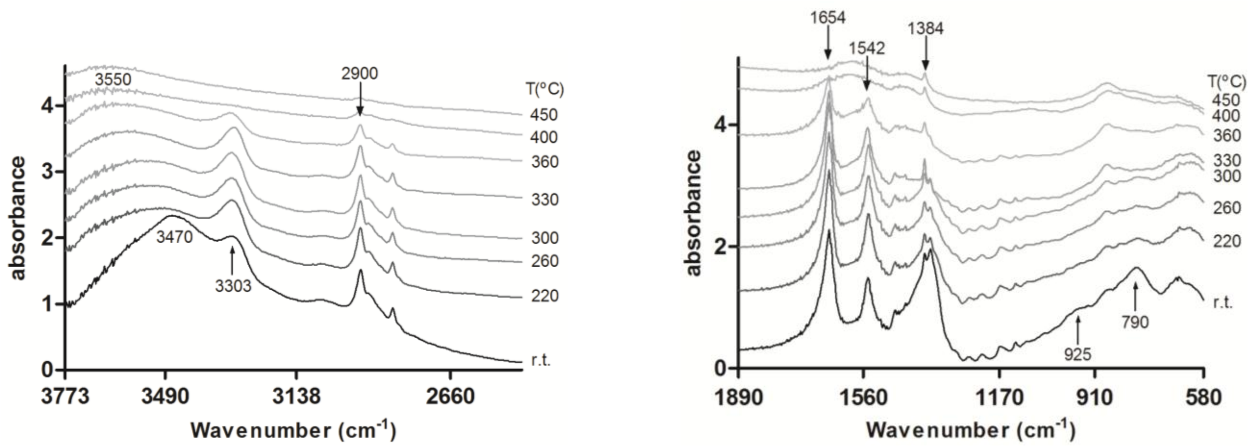

Figure S14 FT-IR at increasing temperature of IPL2$_{60}$.

Table S2 Relationship between areas of amide I and II bands at increasing temperature

PLL3 T (ºC)	Amide I (cm^{-1})	Amide II (cm^{-1})	Amide I/ AmideII	**IPL3** T (ºC)	Amide I (cm^{-1})	Amide II (cm^{-1})	Amide I/ AmideII
60	1.45	0,82	1,76	60	0,28	0,14	1,97
90	1.47	0,82	1,78	90	0,28	0,14	2,01
130	1.51	0,83	1,81	130	0,28	0,14	1,98
170	1.56	0,87	1,81	170	0,28	0,15	1,94
220	1.600	0,87	1,83	220	0,29	0,15	1,93
260	1,60	0,84	1,90	260	0,29	0,15	1,88
300	1,62	0,84	1,90	300	0,29	0,15	1,88
330	1,61	0,86	1,88	330	0,29	0,15	1,89
360	1,46	0,84	1,26	360	0,28	0,15	1,89
400	0,58	0,75	1,93				
PLL2$_{60}$ T (ºC)	Amide I (cm^{-1})	Amide II (cm^{-1})	Amide I/ AmideII	**IPL2$_{60}$** T (ºC)	Amide I (cm^{-1})	Amide II (cm^{-1})	Amide I/ AmideII
60	0,60	0,35	1,72	60	0,16	0,08	2,06
90	0,60	0,35	1,73	90	0,16	0,08	2,08
130	0,61	0,36	1,73	130	0,16	0,08	2,04

170	0,63	0,36	1,73	170	0,16	0,08	2,03
220	0,65	0,37	1,74	220	0,16	0,08	1,99
260	0,67	0,38	1,78	260	0,16	0,09	1,80
300	0,68	0,38	1,79	300	0,16	0,09	1,78
330	0,68	0,37	1,83	330	0,16	0,09	1,74
360	0,66	0,36	1,86	360	0,13	0,07	1,75
400	0,37	0,19	1,94				